Hole in One: an element reduction approach to modeling bone porosity in finite element analysis

Beatriz L Santaella [Corresp., 1] , Z. Jack Tseng [1, 2, 3]

[1] Department of Pathology and Anatomical Sciences, Jacobs School of Medicine and Biomedical Sciences, State University of New York at Buffalo, Buffalo, New York, United States

[2] Department of Integrative Biology and Museum of Paleontology, University of California, Berkeley, Berkeley, California, United States

[3] Division of Paleontology, American Museum of Natural History, New York, New York, United States

Corresponding Author: Beatriz L Santaella
Email address: bsantaella@outlook.com

Finite element analysis has been an increasingly widely applied biomechanical modeling method in many different science and engineering fields over the last decade. In the biological sciences, there are many examples of FEA in areas such as paleontology and functional morphology. Despite this common use, the modeling of trabecular bone remains a key issue because their highly complex and porous geometries are difficult to replicate in the solid mesh format required for many simulations. A common practice is to assign uniform model material properties to whole or portions of models that represent trabecular bone. In this study we aimed to demonstrate that a physical, element reduction approach constitutes a valid protocol for addressing this problem in addition to the wholesale mathematical approach. We tested a customized script for element reduction modeling on five exemplar trabecular geometry models of carnivoran temporomandibular joints, and compared stress and strain energy results of both physical and mathematical trabecular modeling to models incorporating actual trabecular geometry. Simulation results indicate that that the physical, element reduction approach generally outperformed the mathematical approach: physical changes in the internal structure of experimental cylindrical models had a major influence on the recorded stress values throughout the model, and more closely approximates values obtained in models containing actual trabecular geometry than solid models with modified trabecular material properties. In models with both physical and mathematical adjustments for bone porosity, the physical changes exhibit proportionately more weight than material properties changes in approximating values of control models. Therefore, we conclude that for modeling trabecular bone in finite element simulations, maintaining or mimicking the internal porosity of a trabecular structure is recommended as a fast and effective method in place of modification of material property parameters, to better approximate trabecular bone behavior observed in models containing actual trabecular geometry.

1 Hole in One: an element reduction approach to modeling

2 bone porosity in finite element analysis

3

4

5

6 Beatriz L. Santaella[1], Z. Jack Tseng[1,2,3]

7

8 [1]Department of Pathology and Anatomical Sciences, Jacobs School of Medicine and Biomedical

9 Sciences, State University of New York, Buffalo, New York, U.S.A.

10 [2]Department of Integrative Biology and Museum of Paleontology, University of California,

11 Berkeley, California, U.S.A.

12 [3]Division of Paleontology, American Museum of Natural History, New York, New York, U.S.A.

13

14

15

16 Corresponding Author:

17 Beatriz L. Santaella

18

19 Jacobs School of Medicine and Biomedical Sciences, 955 Main St.

20 Buffalo, NY 14203, U.S.A.

21 Email address: bsantaella@outlook.com

22

23

24

25

26

27

28

29

30 Abstract

31

32   Finite element analysis has been an increasingly widely applied biomechanical modeling method
33   in many different science and engineering fields over the last decade. In the biological sciences,
34   there are many examples of FEA in areas such as paleontology and functional morphology.
35   Despite this common use, the modeling of trabecular bone remains a key issue because ~~their~~
36   highly complex and porous ~~geometries are~~ difficult to replicate in the solid mesh format required
37   for many simulations. A common practice is to assign uniform model material properties to
38   whole or portions of models that represent trabecular bone. In this study we aimed to
39   demonstrate that a physical, element reduction approach constitutes a valid protocol for
40   addressing this problem in addition to the wholesale mathematical approach. We tested a
41   customized script for element reduction modeling on five exemplar trabecular geometry models
42   of carnivoran temporomandibular joints, and compared stress and strain energy results of both
43   physical and mathematical trabecular modeling to models incorporating actual trabecular
44   geometry. Simulation results indicate that that the physical, element reduction approach
45   generally outperformed the mathematical approach: physical changes in the internal structure of
46   experimental cylindrical models had a major influence on the recorded stress values throughout
47   the model, and more closely ~~approximates~~ values obtained in models containing actual trabecular
48   geometry than solid models with modified trabecular material properties. In models with both
49   physical and mathematical adjustments for bone porosity, the physical changes exhibit
50   proportionally more weight than material properties changes in approximating values of control
51   models. Therefore, we conclude that for modeling trabecular bone in finite element simulations,
52   maintaining or mimicking the internal porosity of a trabecular structure is recommended as a fast
53   and effective method in place of modification of material property parameters, to better
54   approximate trabecular bone behavior observed in models containing actual trabecular geometry.

Introduction

Finite element analysis (FEA) is a continuum mechanics-based technique originally conceived and used in the engineering design process to predict the behavior (i.e. response) of structures to prescribed loading conditions. This technique uses discretized representations of real-world structures, thereby enabling the design of these systems to be optimized mathematically with minimum physical prototyping and testing (Dumont et al., 2009; Zienkiewicz and Taylor, 2000). With advances in computer software packages that allow a seamless connection of FEA to CAD and image data based modeling, the simulation method has also been applied to functional morphological research in organismal biology, including extinct organisms (as reviewed in Ross, 2005; Rayfield, 2007; Bright, 2014). FEA of feeding mechanics of living and extinct vertebrates have been used in comparative functional morphology for more than a decade (Rayfield, 2005; Alexander, 2006; Barrett and Rayfield, 2006; McHenry et al., 2006; Thomasson et al., 2007), and the method also has been applied in studies in other organismal systems such as insect flight and mechanoreception (Combes and Daniel, 2003; Dechant et al., 2006; Wootton, 2003), and plant biomechanics (Fourcaud and Lac, 2003; Niklas, 1999).

For the last decade or so, the boundaries of FEA have been pushed towards the better modeling of bone structures to better understand skeletal form and function (Rayfield, 2007; Bourke et al., 2008; Wroe et al., 2008; Strait et al., 2010). Still, porous structures like trabecular bone and other complex biological geometries remain problematic in FE modeling given their internal complexity, and the conversion from 2D to 3D of intricate structures that frequently generate errors in elemental overlaps and highly skewed elemental shapes in small anatomical regions. Based on our experience working with bone meshes, biological structures with a high amount of trabecular bone or porous components have higher chances of meshing errors in the FE solid meshing process (but see Fagan et al., 2007 for an alternative, albeit computationally more intensive, and resolution limiting, voxel-based modeling approach). When modeling this type of porous structure, it is common to avoid the complexity of creating a detailed trabecular network by modeling entire models as homogeneous cortical bone and ignoring trabecular geometry, and/or changing the material properties in different element groups within a model to represent cortical versus trabecular bones (Strait et al., 2005, 2009; Wroe, 2008; Attard et al., 2011; Chamoli and Wroe, 2011). This general simplification approach is used in most comparative studies using FEA that incorporate trabecular morphology, even though it has been demonstrated that trabecular structures can play a very important role in the performance of a mesh when using FEA (Parr et al., 2013).

Our objective in this study is to test an alternative, mechanical approach to trabecular bone modeling as a viable solution in addition to mathematical approaches (i.e., changing the material properties of solid models). Potential solutions to accommodate trabecular morphology in finite element modeling that can bypass time-consuming and scan resolution-dependent micro-

95 modeling of trabecular structures are desired. We aim to test the hypothesis that percentage
96 porosity adjustments in solid finite element meshes will generate simulation results comparable
97 or closer to those using actual trabecular morphology, compared to solid models using only
98 modified material property parameter values to simulate trabecular bone behavior.
99

Materials and Methods

101
102 We used five species samples to test a finite element reduction approach to trabecular bone
103 modeling relative to actual trabecular structural models. Each species-specific test sample is
104 represented by three types of experimental cylindrical models: one control cylinder ("CC"); one
105 physically modified cylinder ("PC"); and one material-modified cylinder ("MC"). Definitions of
106 each cylinder model are given below.
107

108 **Control group cylinders**
109 The spongy bone cylinder core meshes were taken from Wysocki and Tseng (2018), based on
110 scans of carnivoran (Carnivora, Mammalia) skull specimens from the American Museum of
111 Natural History (*Arctonyx collaris*; *Bassariscus astutus*; *Enhydra lutris*; *Mellivora capensis*;
112 *Vulpes vulpes*) (see Table S1 for scanning parameters). We emphasize that this is not a full-scale
113 comparative analysis; the species were selected based on the relative fill volume range (the
114 amount of space within a predefined digital cylinder sample of trabecular network within the
115 temporomandibular joints of each species that is space versus those that are bone; Wysocki and
116 Tseng, 2018). Our sample choices allowed testing of each trabecular material modeling method
117 over a relatively wide range of naturally occurring variations in trabecular density. The range of
118 relative fill volumes span from 7.8% porosity (or 92.2% bone) in *Mellivora capensis* to 46.6%
119 porosity (or 53.4% bone) in *Bassariscus astutus*. These specimen-derived cylinders correspond
120 to a control group to serve as a reference for PC and MC model approximations of von Misses
121 stress and total strain energy. Von Mises stress is a good predictor of failure under ductile
122 fracture, and an appropriate metric for comparing the relative strength of models of bones; strain
123 energy is a measure of the work done in deforming a structure, and is a metric of the degree of
124 overall stiffness or degree of deformation of a structure (Dumont et al., 2009).
125

126 Full cylinders corresponding to the maximum, solid volumes possible for the virtual cylindrical
127 cores used in Wysocki and Tseng (2018) were designed in Geomagic Wrap 2017.0.1.19 (3D
128 Systems, Rock Hill, South Carolina) with a 10mm height and 5mm diameter. Ten cylinders were
129 created, five to be modified by physical element reduction to increase porosity, and the other five
130 to be modified in their material properties but not physical geometry (i.e. they remain solid
131 cylinders). When finished, the cylinders were exported as binary stereolithographic files (.stl).
132 These models serve as input for further processing in the finite element simulation software.
133

134 **Material modified cylinder group**

135   We defined the material properties to apply in all the meshes in the CC and PC experimental
136   groups based on values used in numerous previous FEA studies (Young's Modulus: 20 GPa and
137   Poisson's Ratio: 0.3). For the MC group, the Young's Modulus is adjusted within a range (from 7
138   GPa to 22 GPa) that is linearly proportional to the density values of the control cylinder (actual
139   species trabecular geometry) for that experimental group's relative fill volume. Relative fill
140   volume (mm^3) was calculated using the species-derived 3D model that served as the standard
141   (Wysocki and Tseng., 2018). The range was kept in between 7 GPa to 22 GPa in Young's
142   Modulus to fully encompass the range observed for cortical bone in the literature (Cowin, 1989;
143   Erickson et al., 2002). A high porosity physically modified cylinder model (i.e., 46.6% porosity,
144   with 53.4% of the volume being solid) will be associated with a low Young's Modulus (i.e. 7
145   GPa) material modified cylinder model in our study. The remaining boundary conditions for the
146   MC group were set up as in the CC group.
147
148   **Physically modified cylinder group**
149   A set of the solid meshed cylinders were post-processed using a custom script built in R 3.5.1 (R
150   Foundation for Statistical Computing, Vienna, Austria) that created an induced porosity into
151   cylinder models by randomized solid element removal (full script is available at
152   https://github.com/BeaSantaella/Hole-in-One.git). After importing a solid mesh file from Strand7
153   into R, then designating a user-defined amount of tetrahedral deletion (as a percentage), the
154   script goes through all the brick elements (which form the structure modeled, and are formed by
155   individual, four-noded tetrahedral elements) and randomly removes the designated percentage of
156   elements from the model. Each tetrahedral element can be randomly selected for removal only
157   once; in other words, randomized selection of elements for removal is done without replacement.
158   The script output is a text file (.txt) in Strand7 format, which can be read back into the simulation
159   software for further analysis.
160
161   Each script was assigned a percentage of material deletion based on the relative fill volume of
162   their corresponding control group attributes (26.1% for *Arctonyx collaris;* 46.6% for *Bassariscus*
163   *astutus*; 16.5% for *Enhydra lutris*; 7.8% for *Mellivora capensis*; 35.8% for *Vulpes vulpes*).
164
165   **Script Analyses: Does random element reduction deliver consistent results?**
166   Prior to comparing PC models to the CC group or MC group, we tested an additional set of 5
167   models to ascertain the internal consistency of the script (whether random element deletion
168   delivers consistent results).
169
170   We applied the same script, set at 16.5% volume deletion (we chose 16.5% deletion as a mid-
171   range value through our tested range), to five otherwise identical solid cylinder models. The
172   remaining parameter values, such as material properties (Young's Modulus: 20 GPa and
173   Poisson's Ratio: 0.3), the amount of force applied (1,000N), nodes retrained (four nodes, at the
174   end of a cross-section, at the bottom of the cylinder), and the area of application all remained

175   identical (see Model Simulation Parameters). All the points sampled were identical through all of
176   the five cylinders (Fig.1).
177

178   If large differences in magnitude of the stress values are present in script-generated models
179   across different replicates, the script would not represent a true randomized approach to element
180   reduction. If the effects of the script are random, the variability in the results for all 5 additional
181   models should be within comparable ranges of variation. Some variability is expected because
182   the script is based on a random pattern. As a consequence, some arbitrary associations that affect
183   stress values may occur. Overall, our assumption is that replication of porosity in trabecular
184   structures by random reduction of solid element would result in replication of overall trabecular
185   mechanical behavior.
186

187   **Combined Physically modified and Material modified cylinders**
188   In order to assess the joint efficacy of introducing both physical porosity and modification of
189   material property parameters, another set of models was created. They present the same
190   percentage of deletion to corresponding PC models, but their material properties were also
191   adjusted to reflect those of their corresponding MC models.
192

193   **Model Simulation Parameters**
194   We ~~use~~ Finite Element Analysis (FEA) software Strand7 2.4.6 (G1D Computing Pty, Sydney,
195   Australia) to solid mesh the surface cylinder models generated in Geomagic Wrap. In FEA, the
196   geometry of the structural system of interest is approximated by a mesh of simple polyhedral
197   shapes called 'finite elements', connected together at 'nodes', which are the vertices of
198   polyhedra (Dumont et al., 2009). These polyhedra (known as "bricks" in Strand7) constitute a
199   solid mesh filled inward from the triangular faces of the surface mesh that encompass space
200   representing bone (surface meshes were generated in Geomagic Wrap). A mesh formed by bricks
201   is considered a solid mesh, the mesh type used for finite element analysis in the majority of 3D
202   comparative functional morphology studies.
203

204   We applied an arbitrary, 1,000N of force over the nodes on the entire top surface of all cylinder
205   models and recorded nodal stress values (von Mises stress) at four transects in each model. We
206   sampled a total 40 points along the surface of the cylinders (from top to bottom, 10 sampling
207   points per transect). The mean stress values calculated from these nodal transects are used to
208   compare the CC, PC, MC, and PC+MC experimental groups (Fig. 1). For all model categories,
209   total stored strain energy values are also extracted from each simulation run, in order to
210   characterize the overall stiffness or deformation experienced by the models. All analyses were
211   ~~linear~~ static, which means the relationship between the load and the response is linear; and the
212   applied load does not vary with time. Model files for all analyses conducted are available for
213   download at Zendodo (https://doi.org/10.5281/zenodo.3344501).
214

Results

Our results show that physically modified cylinder replicates, assigned the same specific settings, have largely uniform outputs (Fig. 2, Table S2-S3). There was only a small problematic region, located at the bottom (points 8 to 10) of one of the transects in cylinder IV (Fig. 2A, Table S2). Because there are no differences between the cylinders beside the random arrangements that the script may have produced, the higher stress values on the nodes correspond to a more localized deletion at the sampled area. The higher deletion around that area would affect how the applied force is transmitted and distributed in that location, and thereby extend influence to contiguous areas (as subsequent points show higher stress values). This inconsistency effect is diluted by average stress values across analogous locations of the four sampling transects on each cylinder (Fig. 2B, Table S3). Therefore, all subsequent simulated stress values are reported as mean values.

There is a better overall performance of the physically modified cylinders in comparison with material modified cylinders when referring to the control cylinders. In the experimental groups for 26.1% and 46.6% porosity (Fig. 3C, 3E, Tables S6-S8), we see a consistent performance of the PC. We can see a slightly more accurate overall trend in physically modified cylinders (it underestimates in certain regions and it is not able to imitate the peaks of CC, but replicates the general trend). The particular, the bottom section (sampled nodes 8 to 10) of the PC cylinders has a more accurate performance (relative to the control) than the material modified cylinders. MCs in both 26.1% and 46.6% models exhibit a linear transect trend with relatively low stress changes.

On the other hand, in the experimental group of 16.5% porosity (Fig. 3B, Table S5), PC seemed to be unable to correctly replicate both trend and stress values of the control group. For the experimental group of 7.8% porosity (Fig. 3A, Tables S4), PC and MC seem to perform equally well in most of the sampling points (same stress values or off by less than 10 MPa). Except at the beginning and the end (where higher variability may be present, close to the area of force application and nodal restraints), there are minimal differences in stress values across all modeling approaches tested at the lowest porosity level.

In the experimental group of 35.8% porosity (Fig. 3D, Tables S7), the differences in stress values seem to be consistent with what we observe in groups with 26.1% and 46.6% porosity (Fig. 3C and Fig. 3E, Tables S6-S8). PC replicates the overall CC trend but its values are offset by 60 to 80 MPa, especially at the center core region. MC shows a less accurate trend, with a more linear pattern, and even less resemblance to the CC trend. As seen in all experimental groups (Fig. 3A-3E, Tables S4-S8) the combined PC+MC approach presents the same stress values as the PC group results. The differences are indistinguishable between PC and PC+MC results. The overall

254   stress trends relative to porosity changed are plotted separately for the control versus element-
255   reduction models in Figure 4.
256
257   Strain energy values, used here as an overall measure of the stiffness or degree of deformation
258   experienced by the different models, show that when porosity is low, modifying material
259   properties of solid models provides the closest approximation to trabecular geometry models
260   (Fig. 5; Table 1). However, as porosity increases to 16.5% and above, the element reduction
261   models provide the closest approximation to trabecular geometry model strain energy values.
262   Furthermore, a combined modeling approach of element reduction plus material modification
263   generates close approximations of strain energy values at lower porosities, but is less accurate
264   than either material or element reduction approaches alone, in models with higher porosities
265   (Fig. 5).
266

267   Discussion

268
269   Element reduction is potentially a more accurate approach for modeling trabecular stress and
270   strain energy than modification of regional material properties. We tested the hypothesis that,
271   even if they are not 100% replicates of trabecular bone models, porous FE models can at least
272   behave in a comparable way, and provide a closer approximation of mechanical behavior than
273   only modifying overall material property parameters of solid models. Our results indicate that an
274   element reduction approach to modeling bone porosity produced stress magnitudes that are
275   generally closer to values generated from models containing actual trabecular bone geometry,
276   compared to only modifying material properties to simulate bone porosity (Figs. 3-4).
277   Furthermore, element reduction produces models with strain energy values that are comparable
278   to those estimated by trabecular bone and material property modified models at low porosity
279   values, and values that best approximate trabecular bone model outcomes at higher porosity
280   values out of all the modeling approaches tested (Fig. 5).
281
282   Overall, the peaks and valleys of stress in the trabecular geometry models are not well-replicated
283   by alternative modeling approaches. Stress peaks in the transect plot for the control group might
284   be explained by how close the sampled node was to a physical hole or opening on the model
285   surface (in other words, adjacent to an internal porous network) (Fig. 4A). The nodal values may
286   be influenced by elevated stress values associated with such porosity. Thus, creating a cover
287   layer of plate elements, then sampling from that surface, could be one modeling solution to
288   account for the source of that possible noise. This could be considered in further studies, but our
289   goal for this first study was to compare relative performances between the mechanical approach
290   and the mathematical approach (PC vs MC); rather than specifically creating a protocol to mimic
291   actual bone. As apparent from the results, the overall stress magnitude changes, but not the
292   precise stress peaks, are replicated using the element-reduction approach proposed in this study
293   (Fig. 4B).

294

295   It is remarkable that even without a cover of cortical bone (or a thick layer that might

296   homogenize the values at the nodal transect regions) the mechanical modeling approach still has

297   a certain consistency (results are similar in all four experimental groups for PC+MC models).

298   Based on our results, the ability of PC models to approximate stress values in the control group

299   models is best in moderate density models. As shown in Fig. 3D, the overall curvature of the

300   stress sampling transect in the Control model ~~are~~ mimicked by PC, whereas material modified

301   cylinder trends show a low-sensitivity trajectory, indicating that the overall performance of

302   material modified cylinders is less accurate than observed for data in the PC group.

303

304   We note that the element reduction script generated models with holes in a random pattern,

305   whereas the actual species trabecular geometries contain holes surrounding a network of bony

306   struts. As a consequence, PC models are more homogeneous in how they distribute forces. In

307   other words, when compared to the CC group, the PC models perform as a more rigid material.

308   This is probably related to their lack of internal heterogeneity in arrangements or concentration

309   of large pores/bony struts that may not be represented by the mechanical modeling approach.

310   This is another key factor to consider in future research into improving accuracy of trabecular

311   bone modeling in FE simulations.

312

313   It is also quite clear that material properties modified cylinders behave as an even more rigid

314   material than the other two groups. The von Mises stress values, which reflect the likeliness of a

315   certain structure to fail, are apparently lower in MC. This stiffness, or lack of it, may be related

316   to the internal network influence on the overall performance (Parr et al., 2013). Our results point

317   to a plausible explanation to why so many published FE analyses report high stiffness values

318   compared to those known for actual bone: most modeling approaches use a "solid

319   approximation" of trabecular bone, but differences in material distribution, which clearly

320   influences stress estimates as per results in this study, are rarely taken into account.

321

322   Bone tissue can behave as a homogeneous material on a microscale (Muller, 2009) with both

323   individual trabeculae and compact bone having similar material properties (Rho et al., 1993).

324   Therefore, changing material properties to differentiate compact versus trabecular bone may not

325   adequately replicate bone behavior in FE simulations. The adjustment of bone porosity based on

326   the internal density of corresponding trabecular geometry models did better replicating the stress

327   and strain energy values of the control group than MC models (Figs. 3, 5). Accordingly, at k,

328   the change in the material properties is a less effective way to approximate model mechanical

329   behavior than physically reducing the element density of solid mesh models via the

330   randomization approach (Fig. 6).

331

332   In addition, models with both physically introduced porosity and material property changes

333   combined behaved similarly to the models with only introduced porosity, suggesting the

334   dominant role of element reduction in dictating surface mechanical behavior of the cylinder
335   models in our study. This finding could be even more important when considering animals with
336   different amounts of trabecular volume. When modeling low trabecular volumes, such as those
337   in the bones of birds or pterosaurs, the considerations should differ from modeling animals with
338   higher bone densities such as some mammals. Consequently, comparative analysis or
339   paleontological reconstructions should consider the nature of the structure that is being analyzed.
340   An adequate adjustment relative to cortical and trabecular bone ratios when modeling could
341   produce more accurate models that reflect mechanical behavior of trabecular geometries.
342
343   All things considered together, we summarize an important take home message for modeling
344   complex geometries of skeletal elements in general: without element reduction or specific
345   modeling of trabecular morphology, comparative FEA studies that include taxa with a wide
346   range of cortical-to-trabecular bone ratios (e.g. relatively low cortical ratio in vertebrates such as
347   birds and extinct taxa such as pterosaurs) will exhibit larger deviations in both stress and strain
348   energy values than those models that represent morphologies with high cortical ratios. This is an
349   additional source of uncertainty in the modeling protocol that could strongly influence simulation
350   outcomes and thereby, functional morphological inferences made from those simulation results.
351   If close approximation of both stress and strain energy values in finite element simulations
352   involving trabecular structures are of interest, findings from this study demonstrate that an
353   element reduction approach would be preferred over existing material property modification
354   protocols.
355

356   Conclusions

357
358   We demonstrated that an element reduction approach to modeling trabecular structure could
359   more closely simulate behavior of trabecular geometry compared to changing material properties
360   in solid models. Additionally, when element reduction and material property modification
361   methods are combined, the effects of element reduction (i.e., generation of porosity) far
362   outweighs the relative effects of material property modification. We suggest that, unless the
363   complex geometry of trabecular bone is precisely accounted for during the model building
364   process, researchers should first consider modeling the porosity of the material instead of
365   changing material properties. This recommendation is supported by our findings that indicate
366   physical internal porosity generation better approximates mechanical performance (stress and
367   strain energy values) of trabecular structures compared to material property changes. Therefore,
368   we recommend taking into account bone porosity in such a physical manner in biomechanical
369   modeling of complex trabecular bone geometries in comparative functional morphological
370   studies, as a fast and effective way to approximate trabecular geometry, and to alleviate potential
371   biases in ~~finite element modeling protocol towards taxa~~ that exhibit high trabecular bone ratios in
372   their morphology.
373

374   ## Acknowledgments

375

383

384

References

385 References
386
387 Alexander, R.M., 2006. Dinosaur biomechanics. Proc. Roy. Soc. Biol. Sci. Ser. B 273,1849–
388 1855.
389
390 Attard, M.R.G., Chamoli, U., Ferrara, T.L., Rogers, T.L., Wroe, S., 2011. Skull mechanics and
391 implications for feeding behaviour in a large marsupial carnivore guild: the thylacine, Tasmanian
392 devil and spotted-tailed quoll. Journal of Zoology 285 (4), 292–300.
393
394 Barrett, P.M., Rayfield, E.J., 2006. Ecological and evolutionary implications of dinosaur feeding
395 behaviour. Trends Ecol. Evol. 21, 217–224.
396
397 Bourke, J., Wroe, S., Moreno, K., McHenry, C.R., Clausen, P.D., 2008. Effects of gape and tooth
398 position on bite force in the dingo (Canis lupus dingo) using a 3-Dfinite element approach. PLoS
399 One 3, 1–5.
400
401 Bright, J. A., 2014. A review of paleontological finite element models and their validity. Journal
402 of Paleontology, 88(4), 760-769.
403
404 Chamoli, U., Wroe, S., 2011. Allometry in the distribution of material properties and geometry
405 of the felid skull: why larger species may need to change and how they may achieve it. Journal
406 of Theoretical Biology 283 (1), 217–226.
407
408 Combes, S.A., Daniel, T.L., 2003. Into thin air: contributions of aerodynamic and inertial-elastic
409 forces to wing bending in the hawkmoth Manduca sexta. J. Exp.Biol. 206, 2999–3006.
410
411 Cowin, S. C., 1989. Bone Mechanics. Boca Raton, Fla.
412
413 Dechant, H.E., Hossl, B., Rammerstorfer, F.G., Barth, F.G., 2006. Arthropodmechanoreceptive
414 hairs: modeling the directionality of the joint. J. Comp. Physiol. A 192, 1271–1278.
415
416 Dumont, E. R., Grosse, I. R., & Slater, G. J., 2009. Requirements for comparing the performance
417 of finite element models of biological structures. Journal of theoretical biology, 256(1), 96-103.
418
419 Erickson, G. M., Catanese III, J., & Keaveny, T. M., 2002. Evolution of the biomechanical
420 material properties of the femur. The Anatomical Record: An Official Publication of the
421 American Association of Anatomists, 268(2), 115-124.
422
423

424 Fagan, M. J., Curtis, N., Dobson, C. A., Karunanayake, J. H., Kitpczik, K., Moazen, M., ... &
425 O'Higgins, P., 2007, December. Voxel-based finite element analysis-Working directly with
426 microCT scan data. In *Journal of Morphology*, Vol. 268, No. 12, pp. 1071-1071.
427
428 Fourcaud, T., Lac, P., 2003. Numerical modelling of shape regulation and growth stresses in
429 trees I. An incremental static finite element formulation. Trees 19,23–30.
430
431 McHenry, C.R., Clausen, P.D., Daniel, W.J.T., Meers, M.B., Pendharkar, A.,
432 2006.Biomechanics of the rostrum in crocodilians: a comparative analysis using finite-element
433 modeling. The Anat. Rec.: Adv. Integr. Anat. Evol. Biol. 288,827–849.
434
435 Niklas, K.J., 1999. A mechanical perspective on foliage leaf form and function. NewPhytol. 143,
436 19–31.
437
438 Parr, W., Chamoli, U., Jones, A., Walsh, W., & Wroe, S., 2013. Finite element micro-modelling
439 of a human ankle bone reveals the importance of the trabecular network to mechanical
440 performance: new methods for the generation and comparison of 3D models. Journal of
441 biomechanics, 46(1), 200-205.
442
443 Rayfield, E. J., 2005. Aspects of comparative cranial mechanics in the theropod dinosaurs
444 Coelophysis, Allosaurus and Tyrannosaurus. Zoological Journal of the Linnean Society, 144(3),
445 309-316.
446
447 Rayfield, E.J., 2007. Finite element analysis and understanding the biomechanics and evolution
448 of living and fossil organisms. Annual Review of Earth and Planetary Sciences 35, 541–576.
449
450 Ross CF. 2005. Finite element analysis in vertebrate biomechanics. Anat Rec A Discov Mol Cell
451 Evol Biol 283: 253–258.
452
453 Strait, D., Wang, Q., Dechow, P.C., Ross, C.F., Richmond, B.G., Spencer, M.A., Patel,B.A.,
454 2005. Modelling elastic properties in finite element analysis: how much precision is needed to
455 produce an accurate model? The Anatomical Record Part A 283A, 275–287.
456
457 Strait, D.S., Weber, G.W., Neubauer, S., Chalk, J., Richmond, B.G., Lucas, P.W.,Spencer, M.A.,
458 Schrein, C., Dechow, P.C., Ross, C.F., Grosse, I.R., Wright, B.W.,Constantino, P., Wood, B.A.,
459 Lawn, B., Hylander, W.L., Wang, Q., Byron, C., Slice, D.E., Smith, A.L., 2009. The feeding
460 biomechanics and dietary ecology of Australopithecus africanus. Proceedings of the National
461 Academy of Sciences of the United States of America 106, 2124–2129.
462

463 Strait, D.S., Grosse, I.R., Dechow, P.C., Smith, A.L., Wang, Q., Weber, G.W., Neubauer,S.,
464 Slice, D.E., Chalk, J., Richmond, B.G., Lucas, P.W., Spencer, M.A., Schrein, C.,Wright, B.W.,
465 Byron, C., Ross, C.F., 2010. The structural rigidity of the cranium of Australopithecus africanus:
466 implications for diet, dietary adaptations, and the allometry of feeding biomechanics. Anatomical
467 Record: Advances in Integrative Anatomy and Evolutionary Biology 293, 583–593.
468
469 Thomassen, H.A., Gea, S., Maas, S., Bout, R.G., Dirckx, J.J.J., Decraemer, W.F., Povel,G.D.E.,
470 2007. Do Swiftlets have an ear for echolocation? The functional morphology of Swiftlets'
471 middle ears. Hearing Res. 225, 25–37.
472
473 Tseng, Z. J., & Wang, X., 2010. Cranial functional morphology of fossil dogs and adaptation for
474 durophagy in *Borophagus* and *Epicyon* (Carnivora, Mammalia). Journal of Morphology,
475 271(11), 1386-1398.
476
477 Wootton, R., 2003. Finite element analysis, or bent cardboard? Approaches to modelling insect
478 wings. Antenna 27, 310–313.
479
480 Wroe, S., Huber, D.R., Lowry, M., McHenry, C., Moreno, K., Clausen, P., Ferrara,
481 T.L.,Cunningham, E., Dean, M.N., Summers, A.P., 2008. Three-dimensional computer analysis
482 of white shark jaw mechanics: how hard can a great white bite? Journal of Zoology 276, 336–
483 342.
484
485 Wroe, S., 2008. Cranial mechanics compared in extinct marsupial and extant African lions using
486 a finite-element approach. Journal of Zoology 274, 332–339.
487
488 Wysocki, M. A., & Tseng, Z. J. 2018. Allometry predicts trabecular bone structural properties in
489 the carnivoran jaw joint. PloS one, 13(8), e0202824.
490
491 Zienkiewicz, O.C., & Taylor, R.L., 2000. Finite Element Method: vol. 1. The Basis.
492 Butterworth-Heinemann, Oxford.

Figure 1

Locations of boundary conditions on the cylinder models (fixed nodes; force and sample transect).
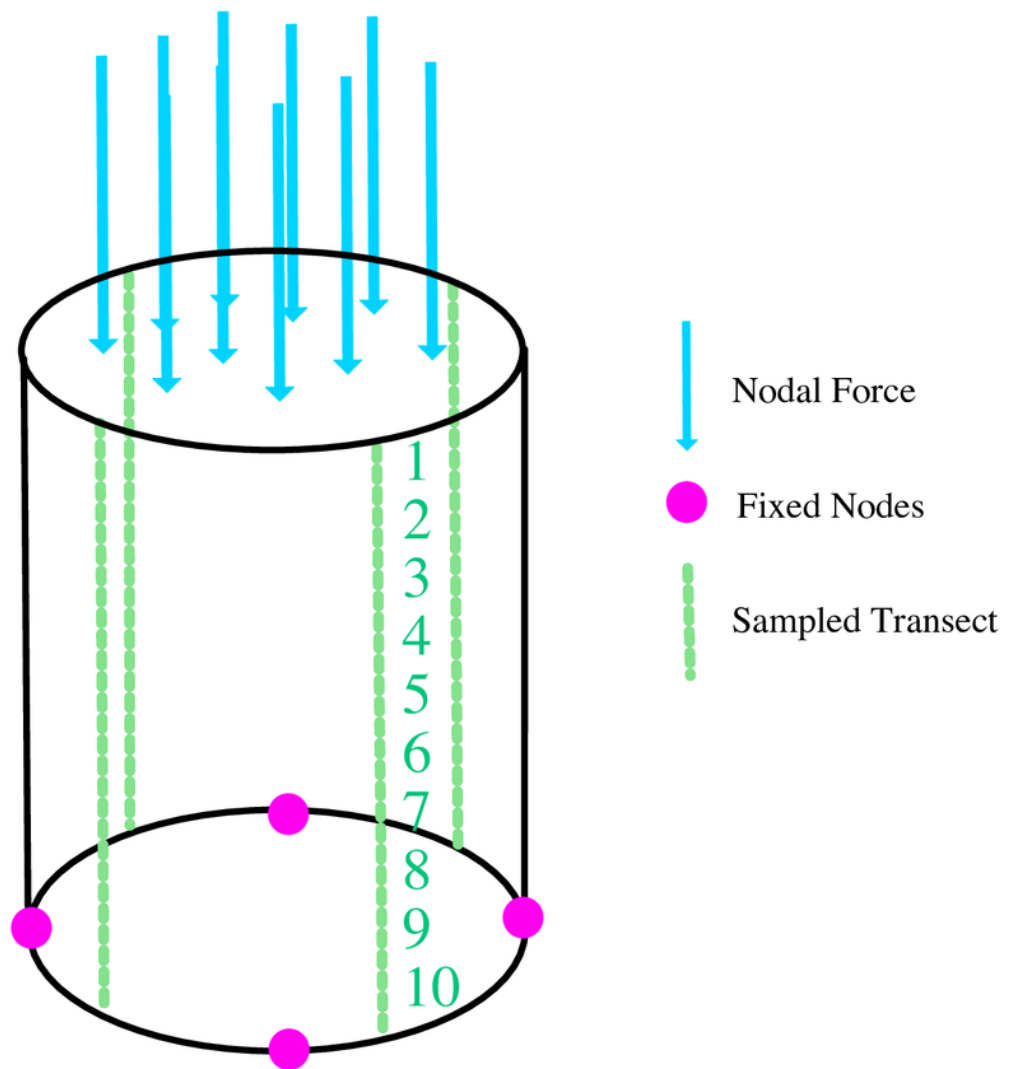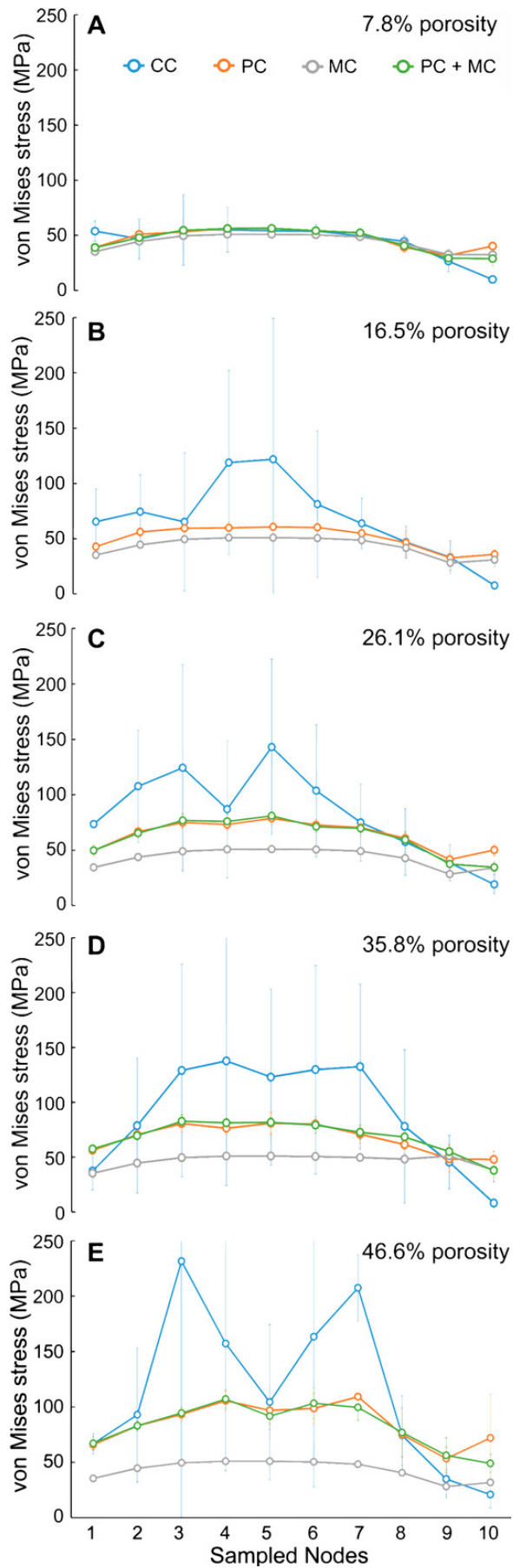
Figure 2

Script Analyses.

Sampled nodes represent 10 equidistant points along data transects where von Mises stress values were recorded (as described in Table S2). The different cylinder model replicates are labeled from I to V. **A**. Stress values obtained from a single transect per replicate. **B**. Mean stress values obtained from four transects taken per replicate. Note the presence of aberrant stress values in replicate IV when sampling a single transect that is averaged out in the four-transect sampling approach.
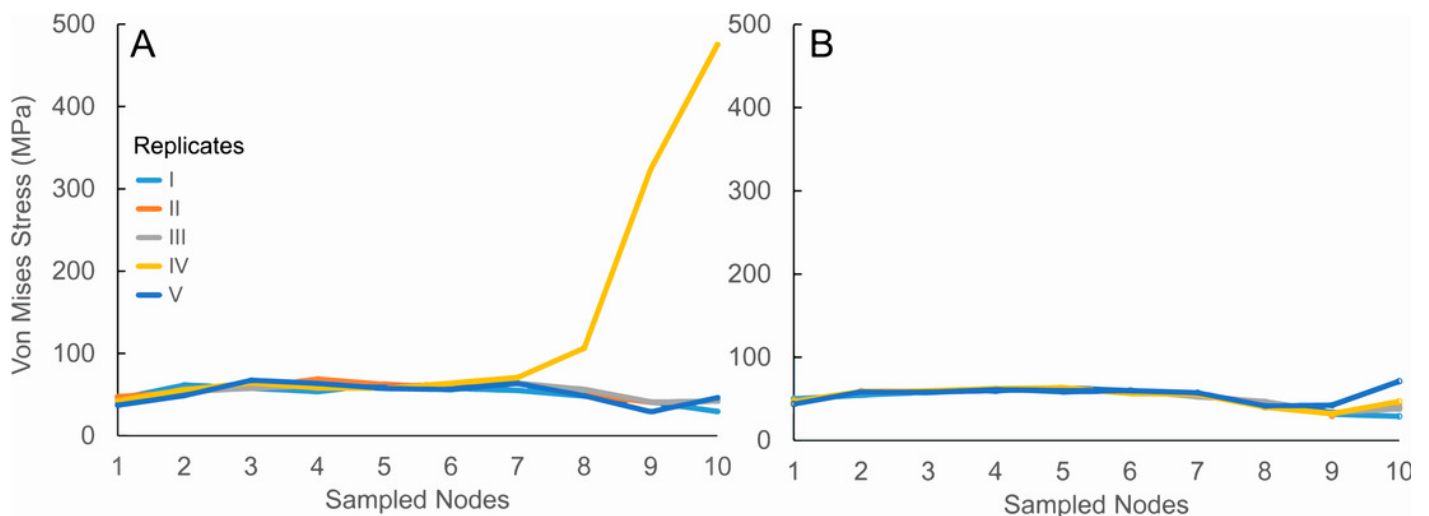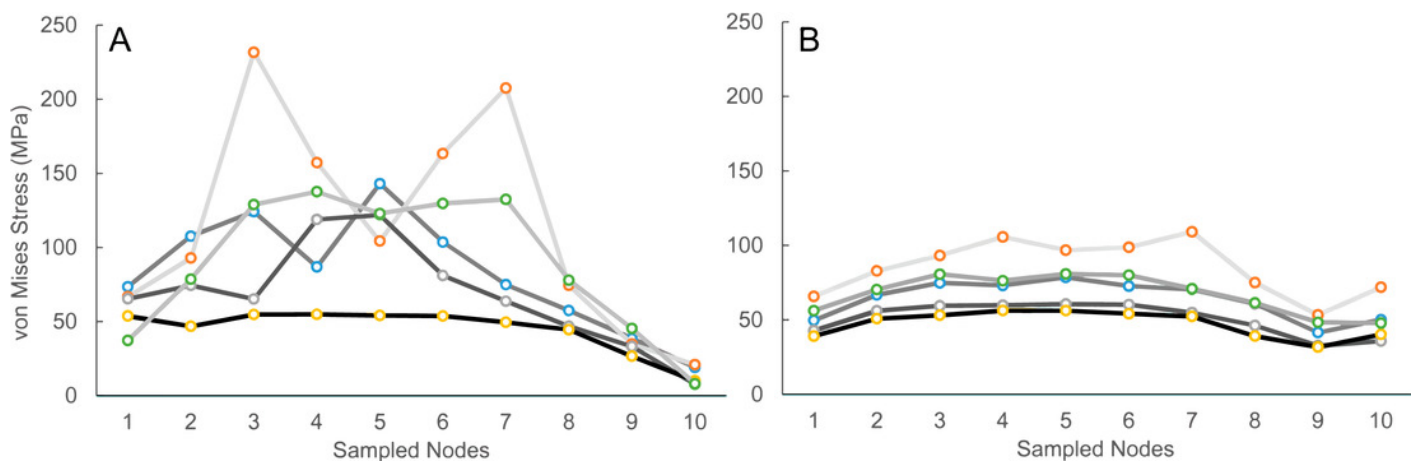
Figure 3

Experimental groups 1 to 5.

On the x-axis, we display 10 points used to collect the data (point 1 top, point 10 bottom). On the y-axis, we show von Mises stress values. Each line is the mean of the four transects sampled (See Tables S4 to S8). The blue line corresponds with the CC; the orange line corresponds with the PC; the grey line corresponds with MC; the green line corresponds with PC+MC. **A** (CC: *Mellivora*; PC: 7.8%; MC: 22GPa), **B** (CC: *Enhydra*; PC: 16.5%; MC: 20GPa), **C** (CC: *Arctonyx*; PC: 26.1%; MC: 16GPa), **D** (CC: *Vulpes*; PC: 35.8%; MC: 10GPa), **E** (CC: *Bassariscus*; PC: 46.6%; MC: 7GPa). Error bars represent 95% confidence intervals around the mean values (See Tables S4 to S8).

Figure 4

von Mises stress values across cylinders, organized by

A. control group results and **B**. element-reduced group results. Degree of porosity is represented by shading of plot lines (darker shade equals lower ~~porosit~~, lighter shade equals higher porosity).

Figure 5

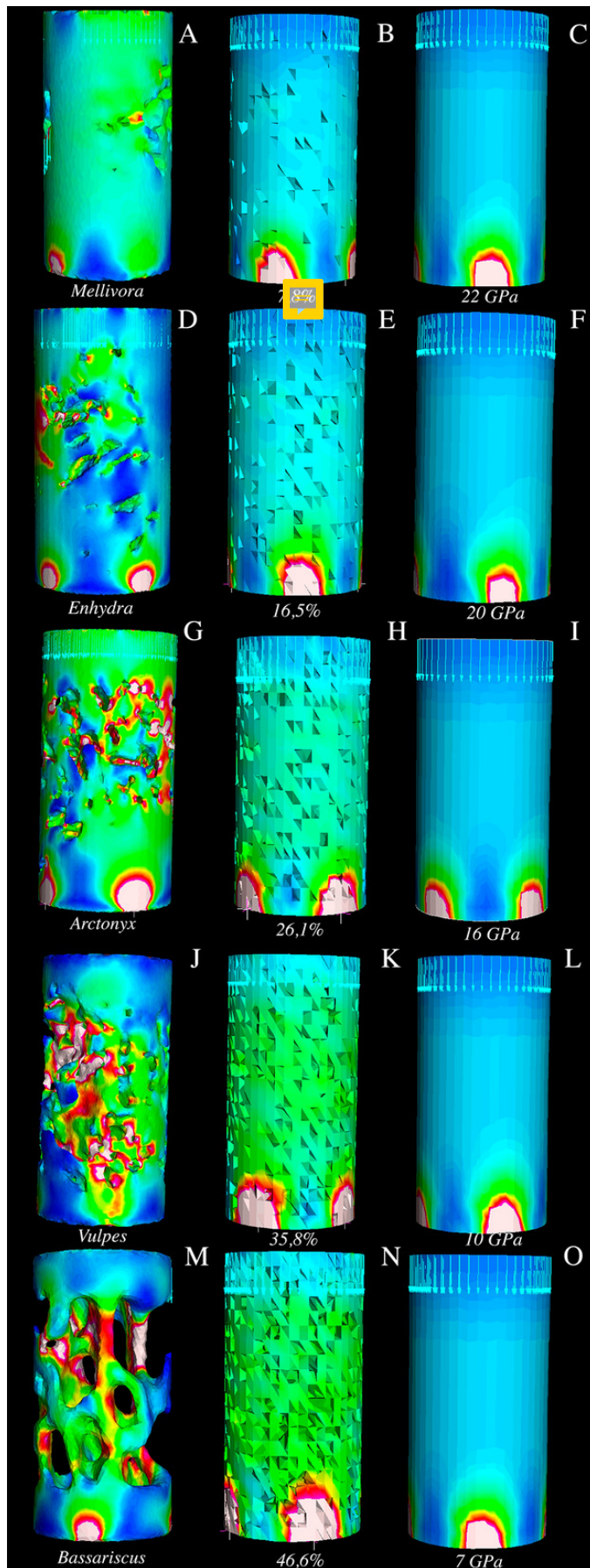Adjusted strain energy comparisons for experimental models.

CC, control group cylinder models; PC, physical element reduction models; MC, material property modified models; J, Joules. For numerical values see Table 1.
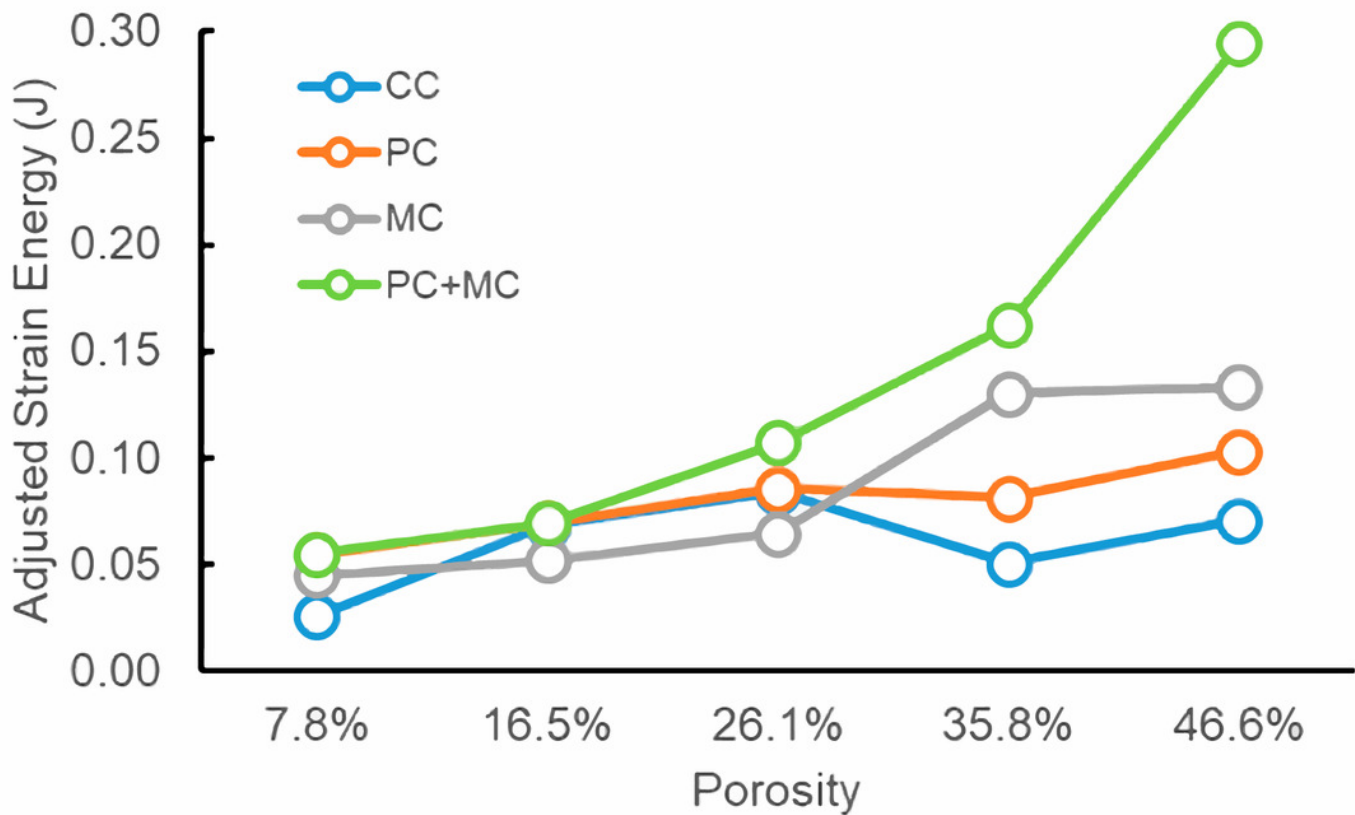
Figure 6

Visualization of von Mises stress in the cylinders.

Vertically the image is separated into three sections (CC, PC, and MC); horizontally the five porosity levels tested are shown. Each cylinder is labeled from A to D.

Table 1(on next page)

Strain energy measurements of experimental models.

CC, control group cylinder models; PC, physical element reduction models; MC, material property modified models; SE, strain energy; ~~J, Joules~~. Raw strain energy values were adjusted by model volume according to the recommendations of Dumont et al. (2009).

1

Porosity	Experiment	SE (J)	Volume (mm3)	Adjusted SE (J)
7.80%	CC	0.0253	180.60	0.0253
	PC	0.0544	180.14	0.0544
	MC	0.0436	195.79	0.0447
	PC+MC	0.0547	180.14	0.0547
16.50%	CC	0.0703	163.51	0.0680
	PC	0.0714	164.07	0.0692
	MC	0.0503	195.79	0.0516
	PC+MC	0.0714	164.07	0.0692
26.10%	CC	0.0902	144.80	0.0838
	PC	0.0921	144.05	0.0855
	MC	0.0629	195.79	0.0646
	PC+MC	0.1151	144.05	0.1068
35.80%	CC	0.0567	125.79	0.0503
	PC	0.0913	125.85	0.0810
	MC	0.1266	195.79	0.1300
	PC+MC	0.1826	125.85	0.1620
46.60%	CC	0.0845	104.71	0.0706
	PC	0.1233	104.94	0.1031
	MC	0.1298	195.79	0.1333
	PC+MC	0.3522	104.94	0.2945

2